

Article

A Novel and Inexpensive Method for Measuring Volcanic Plume Water Fluxes at High Temporal Resolution

Tom D. Pering^{1,*}, Andrew J. S. McGonigle^{1,2,3}, Giancarlo Tamburello^{4,5}, Alessandro Aiuppa^{2,4}, Marcello Bitetto⁴, Cosimo Rubino⁴ and Thomas C. Wilkes¹

¹ Department of Geography, University of Sheffield, Winter Street, Sheffield S10 2TN, UK; a.mcgonigle@sheffield.ac.uk (A.J.S.M.); tcwilkes1@sheffield.ac.uk (T.C.W.)

² Istituto Nazionale di Geofisica e Vulcanologia, Sezione di Palermo, via Ugo La Malfa 153, 90146 Palermo, Italy; aiuppa@unipa.it

³ School of Geosciences, The University of Sydney, Camperdown, NSW 2006, Australia

⁴ DiSTeM, Università di Palermo, via Archirafi, 22, 90123 Palermo, Italy;

giancarlotamburello@gmail.com (G.T.); marcellobitetto@gmail.com (M.B.); c.rubino1991@gmail.com (C.R.)

⁵ Istituto Nazionale di Geofisica e Vulcanologia, sezione di Bologna, Via Donato Creti, 12, 40100 Bologna, Italy

* Correspondence: t.pering@sheffield.ac.uk; Tel.: +44-114-222-7961

Academic Editors: Zhong Lu and Prasad S. Thenkabail

Received: 7 November 2016; Accepted: 6 February 2017; Published: 10 February 2017

Abstract: Water vapour (H₂O) is the dominant species in volcanic gas plumes. Therefore, measurements of H₂O fluxes could provide valuable constraints on subsurface degassing and magmatic processes. However, due to the large and variable concentration of this species in the background atmosphere, little attention has been devoted to monitoring the emission rates of this species from volcanoes. Instead, the focus has been placed on remote measurements of SO₂, which is present in far lower abundances in plumes, and therefore provides poorer single flux proxies for overall degassing conditions. Here, we present a new technique for the measurement of H₂O emissions at degassing volcanoes at high temporal resolution (≈ 1 Hz), via remote sensing with low cost digital cameras. This approach is analogous to the use of dual band ultraviolet (UV) cameras for measurements of volcanic SO₂ release, but is focused on near infrared absorption by H₂O. We report on the field deployment of these devices on La Fossa crater, Vulcano Island, and the North East Crater of Mt. Etna, during which in-plume calibration was performed using a humidity sensor, resulting in estimated mean H₂O fluxes of ≈ 15 kg·s⁻¹ and ≈ 34 kg·s⁻¹, respectively, in accordance with previously reported literature values. By combining the Etna data with parallel UV camera and Multi-GAS observations, we also derived, for the first time, a combined record of 1 Hz gas fluxes for the three most abundant volcanic gas species: H₂O, CO₂, and SO₂. Spectral analysis of the Etna data revealed oscillations in the passive emissions of all three species, with periods spanning ≈ 40 –175 s, and a strong degree of correlation between the periodicity manifested in the SO₂ and H₂O data, potentially related to the similar exsolution depths of these two gases. In contrast, there was a poorer linkage between oscillations in these species and those of CO₂, possibly due to the deeper exsolution of carbon dioxide, giving rise to distinct periodic degassing behaviour.

Keywords: water vapour; passive degassing; infrared cameras; sulphur dioxide; carbon dioxide; remote sensing; UV cameras

1. Introduction

The most abundant volcanic gas species is water vapour (H₂O), which typically constitutes $\approx 79\%$ – 97% of the molar gas composition of released magmatic gases [1]. However, the measurement

of volcanic H₂O fluxes has received relatively little attention to date, mostly due to the large and variable background atmospheric concentrations of this species. This is in contrast to sulphur dioxide (SO₂), which, whilst having far lower plume abundances, is readily resolvable above the trace ambient levels. SO₂ is routinely monitored on volcanoes across the globe, therefore supporting the work of volcano observatories as a tracer for subsurface magmatic conditions [2]. The capturing of H₂O emission rates would be highly desirable, providing better proxies for bulk degassing from volcanoes.

To date, the majority of reported H₂O fluxes have been determined as point values, based on the multiplication of plume-measured H₂O/SO₂ ratios (e.g., from MultiGAS units; [3,4]) by remotely sensed SO₂ fluxes (e.g., from differential optical absorption spectroscopy-DOAS; [5,6]), or ultraviolet (UV) cameras [7,8]. Such data have been derived from locations such as La Fossa crater, Vulcano Island [9], Mt. Etna [10], and the Masaya volcano [11,12]. Other approaches involving thermal imagery and direct sampling have also been employed, on targets such as Vulcano [13], Santa Ana [14], Miyakejima [15], and Satsuma-Iwojima [16].

Recently, a technique based on monitoring the pixel brightness in visible images, to produce uncalibrated high temporal resolution (≈ 1 Hz) time series datasets for H₂O emissions, was devised and applied to the Erebus and Mayon volcanoes [17]. The acquired data captured relatively short-term (few hours) trends in passive degassing from the volcanoes, but are not suitable for monitoring longer-term trends or delivering calibrated emission rate data. Here, we extend this work by reporting on a novel approach for generating high time resolution-calibrated H₂O fluxes based on near infrared (NIR) imagery, using readily available and inexpensive digital cameras. This is the first attempt to provide calibration protocols for uncalibrated visible-NIR absorbance measurements of this species in a volcanic plume. The set-up is related to that already demonstrated in the UV using two bandpass filters, in order to determine SO₂ emission rates from volcanoes (e.g., [7,8,18]). This work also relates to that reported in earlier papers, where single and dual band NIR approaches have been used to characterise the (non-volcanic) water vapour content of the atmosphere, specifically involving “shadow band” instruments and sun photometers [19–22]. In addition to a description of the developed instrumentation, we report on the outcomes of field deployments of these units on the Southern Italian volcanoes: Mt. Etna and Vulcano.

2. Materials and Methods

Two laptop-synchronised Logitech C300 web cameras, each with an 8-bit 1280 × 1024 pixel CMOS sensor, and 64° field-of-view, were co-aligned, side by side. These units were chosen due to their user configurability in terms of acquisition settings. Previous literature studies have also illustrated that this sensor model possesses the detector characteristics required of this application, namely: a linear sensor response [23], and sensitivity in the NIR region (e.g., up to around 1100 nm; [24]), as well as rapid response times (with previously reported application frame rates of up to 15 Hz, as well as detection of femtosecond bursts [23]). A custom Matlab[®] code with a graphical user interface was authored, to operate the cameras in the field. The infrared blocking filter was removed from each camera to avoid absorption of the NIR wavelengths, required for the measurements. The operating principle of this system is similar to that of dual band UV SO₂ cameras (e.g., [7,18]). In particular, we used bandpass filters at 850 nm and 940 nm, where there is a minimum and maximum rate of H₂O absorption, respectively. For further details on the transmission spectra of water vapour in this region, including absorption cross-section data (maximum of ≈ 19 cm²·g⁻¹ for the water vapour molecule around 940 nm), please see reference [25]. The filters were Knight Optical 850FIB12 and 940FIB12, respectively, both of 12.5 mm diameter and 10 nm full-width at half maximum, each of which were mounted to the fore of one of the camera units (transmission curves of each of these filters are available for free download at [26]). During field data acquisitions, the cameras’ exposure settings were controlled to prevent image saturation at 850 nm, whilst ensuring that there was sufficient signal at 940 nm (i.e., after absorption of H₂O in the atmospheric background), leading to typical acquisition frequencies of ≈ 0.2 to 1 Hz. It is worth noting that there is no significant absorption from other

volcanogenic gas species in this wavelength region. In combination with the SO₂ UV camera approach, a vignetting image for each camera was collected, prior to the gas measurements, and all subsequent images acquired with that camera were divided by this vignette image. Vignetting is a common feature of camera systems, caused by light throughput through the filter-lens-aperture system, leading to inhomogeneous illumination of the sensor across the camera's field of view, e.g., [18,27].

An uncalibrated assessment of the H₂O absorption across the camera's field of view was constrained on a pixel-by-pixel basis, following the Lambert-Beer law:

$$a = -\log \left[\frac{\frac{IA_s}{IA_b}}{\frac{IB_s}{IB_b}} \right] \quad (1)$$

where IA and IB refer to the intensities per pixel for filters where H₂O does and does not absorb, respectively. Subscripts s and b refer to the sample (e.g., the plume pixels) and the background, respectively, taken as the average value of a section of the image, adjacent to the plume. This follows the approach which is currently extensively implemented within the volcanology community, in terms of using dual filter UV imaging to measure SO₂ fluxes, following the formalism of Equation (1), as in [7]. Note that we only used the open sky as the background for the measurements in terms of the pixels used in the flux computation, rather than a mixture of pixels, including the foreground (i.e., any plume which may overlap the ground). The combined use of foreground and open sky would induce error.

In combination with the UV camera measurements, this approach is designed to isolate the absorption caused by gas in the volcanic plume, removing attenuation caused by ambient H₂O in the background atmospheric column, in addition to the broadband effects associated with the plume aerosol phase, which apply almost equally to both bands [19].

As a general test of the capacity of this measurement approach to resolve changing levels of atmospheric water vapour, a test was conducted on the water vapour rising from a beaker containing liquid water. This beaker was slowly heated with a Bunsen burner. H₂O absorption was monitored with the camera instrumentation over a ≈ 20 cm path length, through the gases, where ≈ 1.5 W light-emitting diodes at 850 nm and 940 nm, respectively, were used to provide the behind-plume NIR illumination. During the test, the H₂O content (as relative humidity) in the optical path-length was also monitored, using an Extech RHT10 temperature and humidity data logger (Figure 1a shows traces of these parameters throughout the experimental duration). Figure 1b shows a plot of absorbance from Equation (1) vs. the relative humidity values, demonstrating a linear relationship with a good degree of correlation ($r^2 = 0.83$), providing confidence in the capacity of this approach to resolve variable water vapour levels.

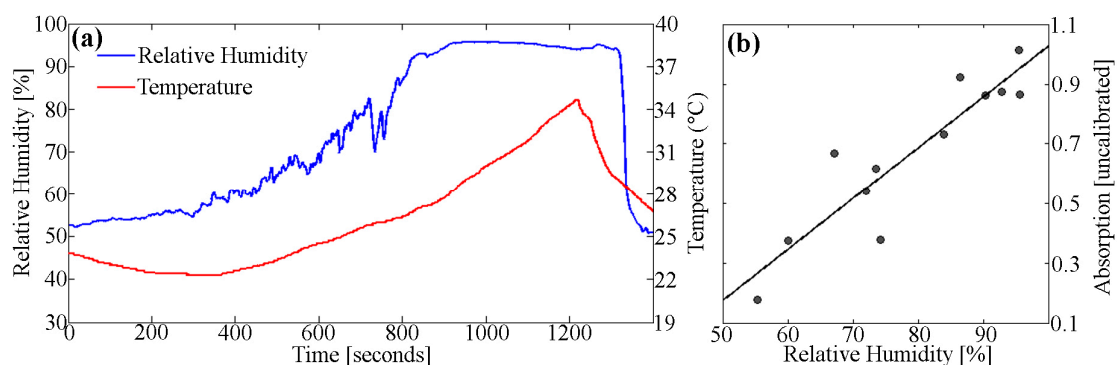


Figure 1. The laboratory proof of the concept detailed in the main text, in which the NIR cameras measured the path-integrated H₂O concentration above a beaker of liquid as it was heated up, where (a) shows the change in temperature and humidity values through time and (b) the camera-derived absorbance is plotted against relative humidity, revealing a linear relationship between these parameters through the heating process.

Note that perfect correspondence could not be expected here as the latter data are path-integrated, but the former are point values, and are thus subject to turbulent effects in the rising “plume”, e.g., even at a fixed temperature, there won’t be a temporally constant humidity value at a fixed point above the beaker. This results in deviations in the humidity data from the general trend of rising values vs. temperature, shown in Figure 1a. Examination of Figure 1a reveals that these random deviations can be up to $\approx 10\%$, which would be sufficient to account for the disparities from the perfect correlation (e.g., where all data points would fall exactly on the line of best fit) in Figure 1b. The manufacturer quoted that error values in the humidity and temperature data logger readings (instrument errors of ± 1 °C and $\pm 3\%$, respectively) will also play a minor role here. Overall, the NIR approach is demonstrated to track changing levels in water vapour as well as could possibly be achieved, given this proof of concept experimental configuration.

3. Results

3.1. Measurements at La Fossa Crater, Vulcano Island

The cameras were deployed on La Fossa crater, Vulcano Island, at position 38.404290°N, 14.960480°E, between the 9 and 11 April 2014, for imaging the fumarolic field degassing. Typical plots of pixel intensity at the two cameras’ wavelengths, in a cross section of the rising plume, are shown in Figure 2a, illustrating the proportionately larger signal attenuation in the 940 nm channel, due to H₂O absorption. Uncalibrated images, providing raw H₂O absorption values, can be used to determine relative changes in uncalibrated H₂O emission magnitudes, which can enable the identification of trends in degassing. Calibration requires establishing a relationship between uncalibrated absorbance in the camera images, and absolute column amounts (i.e., slant column densities) of water. In the case of UV camera SO₂ observations, this is achieved using cells containing known gas concentrations, or by using contemporaneously acquired differential optical absorption spectroscopy (DOAS). Whilst water vapour cells could be used in this application, this would be far more complicated than for SO₂ measurements, given the potential for transitions between the liquid and vapour phase in water. Hence, such a cell mechanism would need to incorporate heating and thermal stabilisation of a liquid water reservoir into a prescribed temperature, previously determined to provide the required vapour density, as well as heating of the cell itself, to avoid condensation. Given the desire to make the system as simple and inexpensive as possible, and to minimise power requirements, this calibration route has not been pursued here. Calibration could also potentially be achieved by using some of the retrieval algorithms previously applied to the determination of precipitable water vapour content in the atmosphere (e.g., [19–22]), or by using Fourier Transform Infrared spectroscopy (e.g., [28]); albeit in the latter case, at rather large instrumental expense. However, both of these approaches would only provide data on the water vapour, rather than the total water content.

In the case of our measurements, we adopted a calibration approach, based on using a low cost humidity sensor (in this case located within a Multi-GAS unit [3,4]) to measure the total H₂O content (e.g., vapour and aerosol phase) as relative humidity, at points within the camera’s field of view, which were readily identifiable within the NIR imagery. On Vulcano, this was achieved by manually portering the humidity sensor to points above individual fumaroles with a GPS receiver, to capture time- and position-stamped water vapour concentrations above individual fumaroles. The acquired data were then converted from relative humidity (RH) values (in %), to ppmv, as follows [9,29]:

$$H_2O[ppmv] = \frac{0.61365 \times e^{17.502 \times T}}{(240.97 + T) \times RH \times 100} \quad (2)$$

where T is the temperature in °C. Following this, the ideal gas law can then be used to convert to absolute humidity in $\text{kg}\cdot\text{m}^{-3}$.

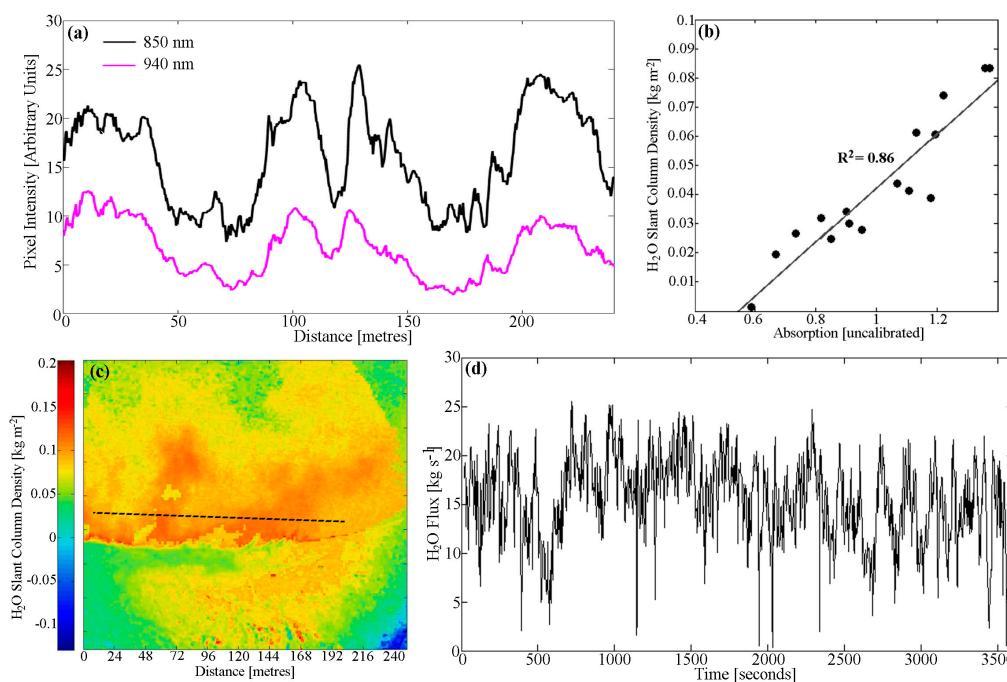


Figure 2. Relating to the field campaign on Vulcano island: (a) an example of pixel intensities from each camera in a horizontal line above the fumarole field degassing, illustrating the greater signal attenuation at 940 nm due to more H₂O absorption than in the 850 nm channel; (b) a system calibration plot of Multi-GAS derived column amounts vs. camera absorbance data points, required to generate calibrated plume imagery; a calibrated image showing slant column densities and ICA line used for (a), is displayed in (c); and in (d) an example flux time series for a one hour acquisition period is shown. See main text for further details.

These absolute humidity values then need to be converted to slant column densities, which are a function of plume depth. In particular, these column densities correspond to the spot gas concentrations integrated over the plume profile, along the field of view of the sensor. In the case of SO₂ UV imaging, where gas cells are used, this problem is not encountered, as the cells contain known column amounts of SO₂ (in units of kg·m⁻²). We tackled this problem in our measurements by measuring water concentrations directly above each fumarole, and taking the width of each “plume” as the distance between the baseline concentrations on opposite sides of these rising plumes, established from the GPS readings during our transects through the fumarole field. The plume profile was taken to be Gaussian, in common with that observed in prior studies on the dispersal of volcanic and non-volcanic plumes, e.g., [28]. Each fumarolic concentration value was then converted to a column amount (i.e., slant column density in kg·m⁻²), by integrating a Gaussian profile of a height equal to this concentration, and of a width equal to the depth, as defined above.

These column amounts were then plotted against the corresponding pixel uncalibrated absorbance from the NIR imagery, as derived from Equation (1), taking into account the effective phase lag of ≈10 s in the humidity sensor readings behind the image-based observations, e.g., the t_{90%} response time of this unit. This resulted in the plot shown in Figure 2b. The pixel values in the uncalibrated absorption images were then multiplied by this gradient, producing the absolute column amount images, e.g., Figure 2c (see supplementary materials for a calibrated image time series video). All of these steps mimic the approaches adopted in the cell-based calibration of UV camera SO₂ slant column determinations. Note, that by using the humidity sensor readings of the total water vapour content, e.g., including the gas and aerosol phase, this enabled the conversion of the uncalibrated water vapour absorption from the imagery, to the total water vapour (e.g., gas and aerosol phase) slant column densities in the plume.

The conversion of H₂O slant column density images to gas fluxes follows the protocols applied in the ultraviolet image sensing of SO₂ fluxes, as more fully documented in the literature [7,8,18]. We firstly defined a horizontal line through the plume, across which integration of the column densities would be performed. The column amounts were then integrated across the plume width, to provide integrated column amounts (ICAs) of water vapour (in kg·m⁻¹). H₂O gas fluxes were finally determined, by multiplying these ICA values by the plume transport speed, which was calculated using the cross correlation technique [30,31]. In summary, this approach involves determining the ICA time series at two distances above the crater terrace, then cross correlating them to determine the inter-series temporal lag, e.g., the time it took for the gas to advect from the lower height, to the higher one. With the knowledge of the spacing between these lines, which is straightforward to ascertain from trigonometry, the plume rise rate is readily determinable. The resulting flux time series for the entire crater terrace, (e.g., Figure 2d) ranged from ≈5 to 25 kg·s⁻¹ (averaging 15 kg·s⁻¹), based on the entire gas flux time series acquisition, from 08:02–14:59 on 11 April 2014. This flux assessment is in reasonable agreement with the previously reported literature values of 6.7 and 2.6 kg·s⁻¹, for two separate days of observations [9].

3.2. Measurements on Mt Etna

The NIR camera units were deployed on Mt. Etna on the 11 September 2013, for the imaging of gas emissions from the North East Crater (NEC) for a period of two hours, from a vantage point at 37.764038°N, 14.993575°E. Uncalibrated absorption images were determined and these were calibrated by means of a humidity sensor, within a Multi-GAS unit placed at a fixed point within the plume on the crater's edge, following the methodology detailed for the Vulcano deployment. In this case, the plume depth was taken as that of the crater's width, and the calibration line gradient was determined by plotting humidity sensor-derived water column amounts vs. contemporaneous uncalibrated absorbances from the NIR camera imagery time series. To consider the emissions from multiple gas species, we employed a UV camera to provide 1 Hz SO₂ fluxes, operated according to the protocols defined in [18], using the Vulcamera software detailed in [32]. Using the method reported in [33], we also combined the UV camera-derived SO₂ fluxes with the Multi-GAS CO₂/SO₂ ratios, in order to calculate 1 Hz CO₂ flux time series.

On the basis of these observations, we present the first contemporaneous record of 1 Hz H₂O, CO₂ and SO₂ gas flux time series from a volcano, in Figure 3a–c. These three multiple gas species time series are referred to as NEC1, NEC2, and NEC3, respectively. Whilst one would not expect an absolute correlation in the emissions of these three species, e.g., a temporal oscillation in released CO₂/SO₂ ratios from Mt. Etna has already been demonstrated [33], there is a degree of correspondence between the manifested peaks and troughs in the species' flux trends. This point is also demonstrated in Figure 4, which shows the SO₂ column amounts averaged over a 10 × 10-pixel section of the UV images, and plotted against the averaged uncalibrated H₂O absorbance in the same field of view, for a series of contemporaneously captured images. In this case, a general relationship is manifested, with scattering about the trend line. One clear deviation from this broad agreement is a pulse in CO₂ degassing at ≈650 s in Figure 3a, which is not manifested in the H₂O dataset, and only marginally in the SO₂ degassing. This mirrors the pulses in CO₂ outgassing, which is not shared in the SO₂ emission dataset, but was noted in an earlier inter-comparison of high time resolution volcanic fluxes of these two gas species [33].

Table 1 displays the minimum, mean, and maximum values for the gas mass ratios, fluxes of the three species, as well as for the overall gas emissions from the NEC, during the entire acquisition period. In particular, the water vapour flux ranged ≈1 to 130 kg·s⁻¹, averaging ≈34 kg·s⁻¹, with an average total gas flux of ≈43 kg·s⁻¹. In comparison, Aiuppa et al. (2008) have reported a water vapour flux of ≈42 kg⁻¹, during a period of quiescent activity at the NEC [10]. The average molar gas composition reported here (e.g., 91%, 7%, and 2%, for H₂O, CO₂, and SO₂, respectively) are in accordance with that expected for magmatic gas release, e.g., within the range of a number of volcanoes, provided in a recent review on this topic (e.g., 79%–97%; 0.5%–12%; 0.2%–6%) [1].

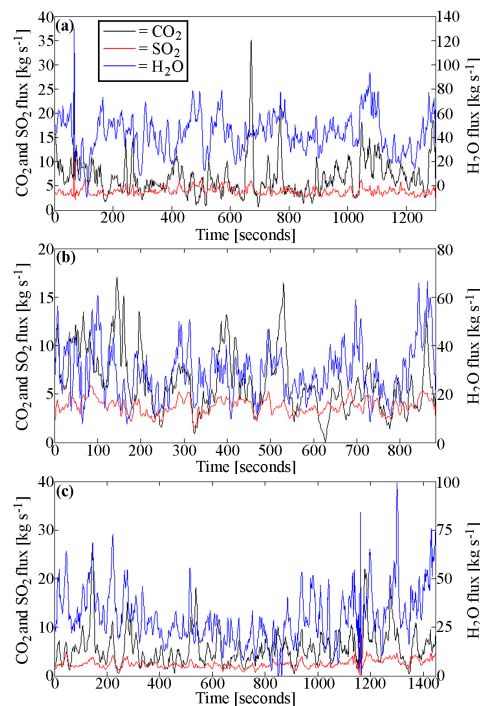


Figure 3. First report of contemporaneous 1 Hz volcanic CO₂, SO₂, and H₂O flux time series; data shown in (a–c) pertain to our observations on the North East Crater for periods: NEC1, NEC2, and NEC3 respectively. At ≈650 s in (a) there is a large spike in CO₂ emission, not evident in the other gases' time series.

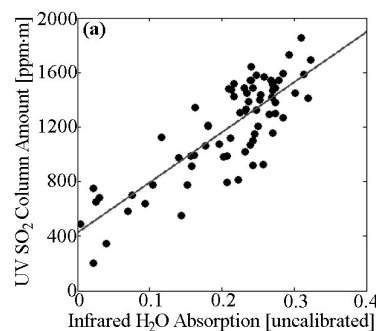


Figure 4. SO₂ column amounts averaged over a 10 × 10 pixel section of the UV images, and plotted against averaged uncalibrated H₂O absorbance in the same field of view, for contemporaneously acquired imagery from the NEC1, 2, and 3 acquisitions, showing a broad correlation about the indicated gradient line.

Table 1. A summary of minimum, mean, and maximum flux ranges in (kg·s⁻¹) for the observations on Mt Etna's North East Crater. The minimum, mean, and maximum mass ratios are reported in addition.

Gas/Ratio	Min	Mean	Max
SO ₂ Flux	1.5	3.4	12
CO ₂ Flux	1	6.3	35
H ₂ O Flux	1	34	130
Total Flux	5	43	180
CO ₂ /SO ₂	0.02	1.9	7.8
H ₂ O/SO ₂	1.7	10.4	23.6
H ₂ O/CO ₂	0.6	7.3	41.8

The acquired data were also subjected to spectral analyses, in order to investigate oscillatory features in the degassing characteristics. In particular, power spectral densities were determined using Welch's method [34] for the acquired time series from the NEC, in order to determine the dominant periods at which oscillatory passive degassing was evident. The results are summarised in Table 2, indicating the presence of periodicities in all three species, on timescales of ≈ 40 –175 s, affirming that passive H₂O emissions are marked by their oscillatory behaviour; noted in earlier works in respect of SO₂ and CO₂ emissions [34–37]. Note that only periods >40 s are reported, in order to avoid oscillations that are potentially attributable to non-volcanogenic causes [37], and Nyquist's criterion is also abided by in terms of the upper limit of oscillations considered here, e.g., up to periods of half the acquisition duration.

Table 2. Periodicities, ranked in order of dominance, manifested in the acquired datasets, derived from power spectral densities using Welch's method. Data from all three separate acquisitions from the North East Crater, e.g., NEC1, 2, and 3 are covered.

Acquisition	Species	Period 1 (s)	Period 2 (s)	Period 3 (s)	Period 4 (s)
NEC1	CO ₂	102	46	-	-
NEC1	H ₂ O	102	56	-	-
NEC1	SO ₂	127	73	56	-
NEC2	CO ₂	73	-	-	-
NEC2	H ₂ O	88	49	-	-
NEC2	SO ₂	109	55	-	-
NEC3	CO ₂	116	77	64	50
NEC3	H ₂ O	175	78	50	-
NEC3	SO ₂	78	64	50	-

4. Discussion

The approach reported here for the measurement of volcanic water vapour fluxes provides the twin benefits of a calibrated gas flux output and a low system cost. This work also builds on that of a previous report on uncalibrated trends in H₂O outgassing, which used a back-scatter-based technique [17], rather than the absorbance measurement adopted here. The potential advantage of working with absorption is that this provides pathlength-integrated information, which may be more representative of the bulk outgassing of the crater, than reflectance values, which pertain to conditions at the front surface of the plume. For future deployments, standalone humidity sensors could be deployed within the instrumental configurations, rather than the Multi-GAS units utilised here, therefore reducing system complexity. In addition, the performance characteristics of this approach could be characterised with respect to summit altitude. As ambient H₂O levels tend to be highest in the lowest sections of the atmosphere, better performance should be achievable on higher volcanoes, where there is stronger incident NIR radiation, and less ambient H₂O, in the upward-looking atmospheric column. Furthermore, given the recent parallel development of smartphone sensor-based UV cameras (also around \approx €500) for volcanic SO₂ flux measurements [38], this could also pave the way for rather inexpensive multiple gas flux data acquisitions from volcanoes, and/or the use of similar camera set-ups, which provide more stable camera operation [39] for the H₂O flux measurements detailed here.

In this work we also captured the first record of contemporaneous 1 Hz gas fluxes for the three most abundant volcanic gas species e.g., H₂O, CO₂, and SO₂ (Figure 3). To further discuss the relevance of these data in volcanology, we investigated the degree to which oscillations in the three gases' emissions, for the NEC observations, were correlated e.g., occurring in phase and at the same frequency. This was achieved using the method detailed in [40], applied to pairs of contemporaneously-acquired gas datasets (e.g., for H₂O and CO₂, SO₂ and CO₂, and H₂O and SO₂). This approach involves performing a continuous wavelet transform [41] on each of the two gases' flux time series, the coefficients from which are then subjected to Spearman's rank correlation analysis, to generate graphical depictions of the degree to

which oscillations at particular periods are shared between the gases (e.g., as shown for the NEC3 data in Figure 5). This revealed a strong correlation between the oscillations of SO₂ and H₂O over almost all of the periods up to that defined by the Nyquist criterion, e.g., as shown in Figure 5c, indicating that these two species, which exsolve at comparable depths, acquire rather similar oscillatory degassing properties. In contrast there is a poorer relationship between the CO₂ periodicity, and that of H₂O and SO₂, particularly in the former case, with a value below 300 s. This is, as might be expected, due to the deeper exsolution of carbon dioxide, leading to different manifested oscillatory degassing behaviour.

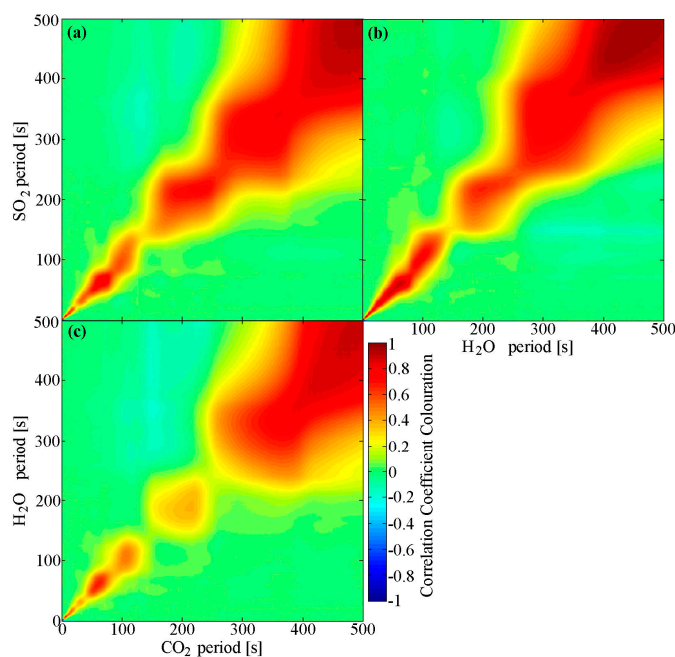


Figure 5. Graphical demonstration of commonality between oscillations in gas fluxes of the three most abundant volcanic gas species: H₂O, CO₂, and SO₂, for observations at the North East Crater of Mt. Etna. These plots were generated from the NEC3 dataset using the technique of Pering et al. (2014) [34], with redder colours representing periods for which oscillations are correlated between the following gas flux pairs; (a) CO₂ and SO₂; (b) H₂O and SO₂; and (c) CO₂ and H₂O.

Whilst volcanic H₂O fluxes provide scope for delivering far better proxies for overall gas release from volcanoes than those of the conventionally-acquired SO₂ emission rate data, consideration needs to be given to the potential non-magmatic origins of such gas emissions, e.g., from meteoric water. On the other hand, whilst SO₂ could be seen to be a more faithful tracer of magmatic conditions in this sense, that species suffers from scrubbing in hydrothermal systems. Therefore, a combined H₂O and SO₂ flux monitoring capability could provide a more holistic gas measurement-based means of gaining insights into magmatic-hydrothermal systems, available from either dataset in isolation. In the case of our Mt. Etna data, we anticipate that the crater plume water vapour fluxes measured here are solely magmatic in origin, as per the previous literature [10], e.g., that the trends in Figure 5 relate purely to magmatic degassing processes. The outgassing from Vulcano is rather more related to hydrothermal interactions [13].

Finally, we also consider the error budget for the determined water fluxes. In terms of random error, we take the standard deviation in the retrieved background sky slant column densities as being representative of this uncertainty in our retrieved plume column amounts per pixel, ΔC , (e.g., [18]), such that $\Delta C \approx \pm 0.03 \text{ kg}\cdot\text{m}^{-2}$. This is around 16% of the maximum slant column values recorded in our observations on Vulcano. In contrast, typical random column amount errors from the literature for UV image-based SO₂ flux determinations, appear to be broadly comparable in percentage terms

(e.g., [38]). In particular, in a previous UV camera determination of gas fluxes from La Fossa crater, with measurements performed at a very similar location to that adopted here, the random error in baseline SO₂ column amounts was around 15% of the maximum recorded value [9]. As all other steps in the flux computation are as per the case of UV SO₂ emission rate determinations, it appears as though random measurement error may be relatively similar in the H₂O and SO₂ cases.

This slant column density error propagates into uncertainty in the integrated column amount (ΔICA), as follows:

$$\Delta ICA = \sqrt{N(\Delta Ch)^2} \quad (3)$$

where N are the number of pixels in the cross section of the plume (i.e., along the line used to determine the ICA) and h is the cross plume width at the plume distance. For our measurements, this translated into a percentage error of around 13% of the mean ICA values. The other major random error source associated with image-based volcanic plume measurements, pertains to the plume speed determination from the cross-correlation method, which is around 10% (e.g., [42]). Based on these factors, and using the La Fossa measurements as an example, we estimate an indicative random water emission rate error from this approach of $\approx \pm 16\%$, based on the root of the sum of the squares of these two individual error sources. This is rather similar to overall assessments of gas flux error in the UV SO₂ observations, as previously reported in the literature [43].

There is also the potential for systematic errors. For instance, light dilution, which is a known issue in UV SO₂ imaging, can cause an underestimation of measured gas fluxes, due to the scattering of photons into the sensor field of view, between the camera and the plume [44]. Whilst the exact quantification of this effect is beyond the scope of this article, light dilution ought to be rather less problematic in the NIR H₂O case, given that Rayleigh scattering is less pronounced at longer wavelengths. There is, furthermore, potential for systematic error in the plume width. For measurements further from the source than performed here, this could be mitigated by using scanning spectrometer observations [45,46] to experimentally measure the plume width at the measurement location.

5. Conclusions

Here, we report for the first time on an inexpensive approach for the high time resolution (1 Hz) capture of volcanic H₂O fluxes. This was achieved on the basis of consumer digital cameras, with an overall system cost of $\approx \text{€}500$, including the required ancillary bandpass filters and the humidity sensor used for calibration. The low cost of these devices enables image-based volcanic gas flux assessments at a far more modest cost than hitherto achievable, with scientific grade UV cameras (e.g., [7,8]), and provides scope for more representative single species gas flux assessment of volcanic outgassing than available from SO₂ data. However, when combined with low cost UV cameras, there is considerable scope for contemporaneous assessment of multiple gas fluxes. The method was field tested at La Fossa crater, Vulcano Island, and the North East Crater of Mt. Etna, where successful calibration of the system to deliver H₂O fluxes was demonstrated, based on in plume measurements of relative humidity, generating flux values in keeping with those previously reported in the literature, e.g., $\approx 15 \text{ kg}\cdot\text{s}^{-1}$ and $\approx 34 \text{ kg}\cdot\text{s}^{-1}$, respectively. By combining our H₂O flux sensor with UV camera and Multi-GAS readings, we also produced the first combined 1 Hz record of the fluxes for the three most abundant volcanic gas species: CO₂, SO₂, and H₂O. Oscillations in the degassing of all three species were identified in the range of $\approx 40\text{--}175 \text{ s}$, with a strong correspondence between manifested fluctuations in the SO₂ and H₂O data, possibly as a result of the similar exsolution depths of those species. In contrast, there is poorer linkage between the oscillations of these gases and those in CO₂, perhaps due to the deeper exsolution of carbon dioxide, leading to establishment of rather different periodic degassing behaviour. This proof of concept study now paves the way for the capture and analysis of longer term multiple gas flux datasets, in tandem with seismic observations, to further

investigate the implications of this oscillatory behaviour for gas flow dynamics on Etna and other low viscosity magmatic systems.

Supplementary Materials: The following are available online at www.mdpi.com/2072-4292/9/2/146/s1, Video S1: Calibrated H₂O flux at Vulcano on the 11 April 2013. This movie spans the ≈1 h data acquisition shown in Figure 2. Note that the colouration in the image corners is not related to vignetting, but the edges of the filters, which overlapped the field of view at the widest look angles. This could be mitigated in the future with wider diameter filters. Changes in image brightness are related to changing illumination, and hence adjustment of exposure time. As the retrieval involves in-image background sky measurements, the latter issue is automatically accounted for in the analysis. The images show relative graininess and dark pixels above the plume related to the relatively inexpensive nature of the acquired camera unit. These issues didn't affect the image-based flux computation, however, as the ICA line was drawn below the pixels in question. We also include a supplementary "kmz" Google Earth file, Location S1, which provides UV camera location data.

Acknowledgments: T.D. Pering acknowledges the support of a NERC studentship (NE/K500914/1), the University of Sheffield, and funds from an ESRC Impact Acceleration Grant. A.J.S. McGonigle acknowledges a Leverhulme Trust Research Fellowship (RF-2016-580). A. Aiuppa, and G. Tamburello acknowledge support from the European Research Council starting independent research grant (agreement 305377). We thank Fred Prata, Loïc Vanderkluysen and two anonymous reviewers for their insightful remarks, which have helped us greatly improve this article.

Author Contributions: T.D.P. and A.J.S.M. wrote the manuscript. T.D.P., G.T., A.A., M.B., and C.R., conducted the fieldwork. T.C.W. provided help with data analysis.

Conflicts of Interest: The authors declare no conflict of interest. The founding sponsors had no role in the design of the study; in the collection, analyses, or interpretation of data; in the writing of the manuscript, and in the decision to publish the results.

References

1. Fischer, T.P.; Chiodini, G. Volcanic, Magmatic and Hydrothermal Gases. In *The Encyclopedia of Volcanoes*, 2nd ed.; Sigurdsson, H., Houghton, B., McNutt, S.R., Rymer, H., Stix, J., Eds.; Academic Press: London, UK, 2015; pp. 779–798.
2. Burton, M.R.; Prata, F.; Platt, U. Volcanological applications of SO₂ cameras. *J. Volcanol. Geotherm. Res.* **2015**, *300*, 2–6. [[CrossRef](#)]
3. Aiuppa, A.; Federico, C.; Paonita, A.; Giudice, G.; Valenza, M. Chemical mapping of a fumarolic field: La Fossa Crater, Vulcano Island (Aeolian Islands, Italy). *Geophys. Res. Lett.* **2005**, *13*. [[CrossRef](#)]
4. Shinohara, H. A new technique to estimate volcanic gas composition: Plume measurements with a portable multi-sensor system. *J. Volcanol. Geotherm. Res.* **2005**, *143*, 319–333. [[CrossRef](#)]
5. McGonigle, A.J.S.; Oppenheimer, C.; Galle, B.; Mather, T.A.; Pyle, D.M. Walking traverse and scanning DOAS measurements of volcanic gas emission rates. *Geophys. Res. Lett.* **2002**, *29*. [[CrossRef](#)]
6. Galle, B.; Oppenheimer, C.; Geyer, A.; McGonigle, A.J.S.; Edmonds, M.; Horrocks, L. A miniaturized ultraviolet spectrometer for remote sensing of SO₂ fluxes: A new tool for volcano surveillance. *J. Volcanol. Geotherm. Res.* **2003**, *119*, 241–254. [[CrossRef](#)]
7. Mori, T.; Burton, M. The SO₂ camera: A simple, fast and cheap method for ground-based imaging of SO₂ in volcanic plumes. *Geophys. Res. Lett.* **2006**, *33*. [[CrossRef](#)]
8. Bluth, G.J.S.; Shannon, J.M.; Watson, I.M.; Prata, A.J.; Realmuto, V.J. Development of an ultra-violet digital camera for volcanic SO₂ imaging. *J. Volcanol. Geotherm. Res.* **2007**, *161*, 47–56. [[CrossRef](#)]
9. Tamburello, G.; Kantzas, E.P.; McGonigle, A.J.S.; Aiuppa, A.; Giudice, G. UV camera measurements of fumarole field degassing (La Fossa crater, Vulcano Island). *J. Volcanol. Geotherm. Res.* **2011**, *199*, 47–52. [[CrossRef](#)]
10. Aiuppa, A.; Giudice, G.; Gurrieri, S.; Liuzzo, M.; Burton, M.; Caltabiano, T.; McGonigle, A.J.S.; Salerno, G.; Shinohara, H.; Valenza, M. Total volatile flux from Mount Etna. *Geophys. Res. Lett.* **2008**, *35*. [[CrossRef](#)]
11. Burton, M.R.; Oppenheimer, C.; Horrocks, L.A.; Francis, P.W. Remote sensing of CO₂ and H₂O emission rates from Masaya volcano, Nicaragua. *Geology* **2000**, *28*, 915–918. [[CrossRef](#)]
12. Martin, R.S.; Sawyer, G.M.; Spampinato, L.; Salerno, G.G.; Ramirez, C.; Ilyinskaya, E.; Witt, M.L.I.; Mather, T.A.; Watson, I.M.; Phillips, J.C.; et al. A total volatile inventory for Masaya Volcano, Nicaragua. *J. Geophys. Res. Solid Earth* **2010**, *115*. [[CrossRef](#)]

13. Bukumirovic, T.; Italiano, F.; Nuccio, P.M. The evolution of a dynamic geological system: The support of a GIS for geochemical measurements at the fumarole field of Vulcano, Italy. *J. Volcanol. Geotherm. Res.* **1997**, *79*, 253–263. [[CrossRef](#)]
14. Witter, J.B.; Hernandez, P.; Harris, A.J.L.; Pérez, N. Quantification of the Mass Flux of H₂O Gas (Steam at Three Active Volcanoes Using Thermal Infrared Imagery. *Pure Appl. Geophys.* **2012**, *169*, 1875–1889. [[CrossRef](#)]
15. Matsushima, N. H₂O emission rate by the volcanic plume during the 2000–2002 Miyakejima volcanic activity. *Geophys. Res. Lett.* **2005**, *32*. [[CrossRef](#)]
16. Matsushima, N.; Kazahaya, K.; Saito, G.; Shinohara, H. Mass and heat flux of volcanic gas discharging from the summit crater of Iwodate volcano, Satsuma Iwojima, Japan, during 1996–1999. *J. Volcanol. Geotherm. Res.* **2003**, *126*, 285–301. [[CrossRef](#)]
17. Girona, T.; Costa, F.; Taisne, B.; Aggangan, B.; Ildefonso, S. Fractal degassing from Erebus and Mayon volcanoes revealed by a new method to monitor H₂O emission cycles. *J. Geophys. Res. Solid Earth* **2015**, *120*, 2988–3002. [[CrossRef](#)]
18. Kantzas, E.P.; McGonigle, A.J.S.; Tamburello, G.; Aiuppa, A.; Bryant, G. Protocols for UV camera volcanic SO₂ measurements. *J. Volcanol. Geotherm. Res.* **2010**, *194*, 55–60. [[CrossRef](#)]
19. Brooks, D.R.; Mims, F.M., III; Roettger, R. Inexpensive near-IR sun photometer for measuring total column water vapour. *J. Atmos. Ocean. Technol.* **2007**, *24*, 1268–1276. [[CrossRef](#)]
20. Michalsky, J.J.; Liljegren, J.C.; Harrison, L.C. A comparison of sun photometer derivations of total column water vapor and ozone to standard measures of same at the Southern Great Plains Atmospheric Radiation Measurement site. *J. Geophys. Res. Atmos.* **1995**, *100*, 25995–26003. [[CrossRef](#)]
21. Halthore, R.N.; Eck, T.F.; Holben, B.N.; Markham, B.L. Sun photometric measurements of atmospheric water vapor column abundance in the 940-nm band. *J. Geophys. Res. Atmos.* **1997**, *102*, 4343–4352. [[CrossRef](#)]
22. Prata, A.J. *Precipitable Water Retrieval from Multi-Filter Rotating Shadowband Radiometer Measurements*; CSIRO Atmospheric Research Technical Paper No. 47; CSIRO: Victoria, Australia, 2000.
23. Cignoli, F.; De Iuliis, S.; Zizak, G. A Webcam as a Light Probe Beam Profiler. *Appl. Spectrosc.* **2004**, *58*, 1372–1375. [[CrossRef](#)] [[PubMed](#)]
24. Langer, G.; Hochreiner, A.; Burgholzer, P.; Berer, T. A webcam in Bayer-mode as a light beam profiler for the near infra-red. *Opt. Lasers Eng.* **2013**, *51*, 571–575. [[CrossRef](#)] [[PubMed](#)]
25. Barducci, A.; Guzzi, D.; Marcoionni, P.; Pippi, M. Algorithm for the retrieval of columnar water vapour from hyperspectral remotely sensed data. *Appl. Opt.* **2004**. [[CrossRef](#)]
26. Knight Optical. Available online: <http://www.knightoptical.com> (accessed on 10 February 2017).
27. Kern, C.; Werner, C.; Elias, T.; Sutton, A.J.; Lübcke, P. Applying UV cameras for SO₂ detection to distant or optically thick volcanic plumes. *J. Volcanol. Geotherm. Res.* **2013**, *262*, 80–89. [[CrossRef](#)]
28. Vance, A.; McGonigle, A.J.S.; Aiuppa, A.; Stith, J.L.; Turnbull, K.; von Glasow, R. Ozone depletion in tropospheric volcanic plumes. *Geophys. Res. Lett.* **2010**, *37*. [[CrossRef](#)]
29. Jensen, M.E.; Burman, R.D.; Allen, R.G. *Evapotranspiration and Irrigation Water Requirements*; ASCE Manuals and Reports on Engineering Practice No. 70; American Society of Civil Engineers: New York, NY, USA, 1990.
30. McGonigle, A.J.S.; Hilton, D.R.; Fischer, T.P.; Oppenheimer, C. Plume velocity determination for volcanic SO₂ flux measurements. *Geophys. Res. Lett.* **2005**, *32*. [[CrossRef](#)]
31. Williams-Jones, G.; Horton, K.A.; Elias, T.; Garbeil, H.; Mouginiis-Mark, P.J.; Sutton, A.J.; Harris, A.J.L. Accurately measuring volcanic plume velocity with multiple UV spectrometers. *Bull. Volcanol.* **2006**, *68*, 328–332. [[CrossRef](#)]
32. Tamburello, G.; Kantzas, E.P.; McGonigle, A.J.S.; Aiuppa, A. Vulcamera: A program for measuring volcanic SO₂ using UV cameras. *Ann. Geophys.* **2011**, *54*, 219–221.
33. Pering, T.D.; Tamburello, G.; McGonigle, A.J.S.; Aiuppa, A.; Cannata, A.; Giudice, G.; Patanè, D. High time resolution fluctuations in volcanic carbon dioxide degassing from Mount Etna. *J. Volcanol. Geotherm. Res.* **2014**, *270*, 115–121. [[CrossRef](#)]
34. Welch, P.D. The Use of Fast Fourier Transform for the Estimation of Power Spectra: A Method Based on Time Averaging Over Short, Modified Periodograms. *IEEE T. Audio Electroacoust.* **1967**, *AU-15*, 70–73. [[CrossRef](#)]
35. McGonigle, A.J.S.; Aiuppa, A.; Ripepe, M.; Kantzas, E.P.; Tamburello, G. Spectroscopic capture of 1 Hz volcanic SO₂ fluxes and integration with volcano geophysical data. *Geophys. Res. Lett.* **2009**, *36*. [[CrossRef](#)]

36. Boichu, M.; Oppenheimer, C.; Tsanev, V.; Kyle, P.R. High temporal resolution SO₂ flux measurements at Erebus volcano, Antarctica. *J. Volcanol. Geotherm. Res.* **2010**, *190*, 325–336. [[CrossRef](#)]
37. Tamburello, G.; Aiuppa, A.; McGonigle, A.J.S.; Allard, P.; Cannata, A.; Giudice, G.; Kantzas, E.P.; Pering, T.D. Periodic volcanic degassing behavior: The Mount Etna example. *Geophys. Res. Lett.* **2013**, *40*, 4818–4822. [[CrossRef](#)]
38. Wilkes, T.C.; Pering, T.D.; McGonigle, A.J.S.; Tamburello, G.; Willmott, J.R. A Low-Cost Smartphone Sensor-Based UV Camera for Volcanic SO₂ Emission Measurements. *Remote Sens.* **2017**, *9*. [[CrossRef](#)]
39. Wilkes, T.C.; McGonigle, A.J.S.; Pering, T.D.; Taggart, A.J.; White, B.S.; Bryant, R.G.; Willmott, J.R. Ultraviolet Imaging with Low Cost Smartphone Sensors: Development and Application of a Raspberry Pi-Based UV Camera. *Sensors* **2016**, *16*. [[CrossRef](#)] [[PubMed](#)]
40. Pering, T.D.; Tamburello, G.; McGonigle, A.J.S.; Hanna, E.; Aiuppa, A. Correlation of oscillatory behaviour in Matlab using wavelets. *Comput. Geosci.* **2014**, *70*, 206–212. [[CrossRef](#)]
41. Grinstead, A.; Moore, J.C.; Jevrejeva, S. Application of the cross wavelet transform and wavelet coherence to geophysical time series. *Nonlinear Proc. Geoph.* **2004**, *11*, 561–566. [[CrossRef](#)]
42. Lübcke, P.; Bobrowski, N.; Illing, S.; Kern, C.; Alvarez Nieves, J.M.; Vogel, L.; Zielcke, J.; Delgado Gradados, H.; Platt, U. On the absolute calibration of SO₂ cameras. *Atmos. Meas. Tech.* **2013**, *6*, 677–696. [[CrossRef](#)]
43. Holland, A.S.P.; Watson, I.M.; Phillips, J.C.; Caricci, L.; Dalton, M.P. Degassing processes during lava dome growth: Insights from Santiaguito lava dome, Guatemala. *J. Volcanol. Geotherm. Res.* **2011**, *202*, 153–166. [[CrossRef](#)]
44. Champion, R.; Delgado-Granados, H.; Mori, T. Image based correction of the light dilution effect for SO₂ camera measurements. *J. Volcanol. Geotherm. Res.* **2015**, *300*, 48–57. [[CrossRef](#)]
45. McGonigle, A.J.S.; Oppenheimer, C.; Hayes, A.R.; Galle, B.; Edmonds, M.; Caltabiano, T.; Salerno, G.; Burton, M.; Mather, T.A. Sulphur dioxide fluxes from Mount Etna, Vulcano, and Stromboli measured with an automated scanning ultraviolet spectrometer. *J. Geophys. Res.* **2003**, *108*, 2455. [[CrossRef](#)]
46. Galle, B.; Johansson, M.; Rivera, C.; Zhang, Y.; Kihlman, M.; Kern, C.; Lehmann, T.; Platt, U.; Arellano, S.; Hidalgo, S. Network for observation of volcanic and atmospheric change (NOVAC)—A global network for volcanic gas monitoring: Network layout and instrument description. *J. Geophys. Res.* **2010**, *115*, D05304. [[CrossRef](#)]



© 2017 by the authors; licensee MDPI, Basel, Switzerland. This article is an open access article distributed under the terms and conditions of the Creative Commons Attribution (CC BY) license (<http://creativecommons.org/licenses/by/4.0/>).